

Cluster Association for 3D Environment Based on 60 GHz Indoor Channel Measurements

Hang Mi^{*†}, Bo Ai^{*}, Ruisi He^{*}, Raied Caromi[‡], Jian Wang[‡], Anuraag Bodi[§],
Camillo Gentile[‡], Yang Miao[†]

^{*} State Key Laboratory of Rail Traffic Control and Safety, Beijing Jiaotong University, Beijing, 100044, China

[†] EEMCS faculty, University of Twente, Enschede, the Netherlands

[‡] Wireless Networks Division, National Institute of Standards and Technology, Gaithersburg, MD 20899 USA

[§] Associate, National Institute of Standards and Technology, Prometheus Computing LLC, Gaithersburg, MD, USA

Abstract—In this paper, we present a ray tracing (RT) assisted multipath cluster association method. This work is based on an indoor channel measurement at 60 GHz, where a light detection and ranging (LiDAR) sensor was co-located with channel sounder and time-synchronized point cloud was captured to describe environmental information. Based on the point cloud, a 3D environment is reconstructed and fed into RT simulation. Then multipath components (MPCs) estimated from the measured channel and that from the RT are clustered, respectively. A novel cluster association algorithm is then proposed to associate the clusters between the measurements and RT. The interaction objects in the 3D environment can be found through this association. From cluster association results, we can better understand the relationship between measured radio channel, environment, and channel characteristics in an automatic manner. As an example, the indoor multi-bounce scattering and composite channel parameters are investigated.

Index Terms—Radio propagation channel, multipath clustering, association, millimeter-wave, ray tracing.

I. INTRODUCTION

Beyond 5G and towards 6G, radio communication systems are envisioned to continue using millimeter-Wave (mmWave) frequencies and up to sub-THz frequencies [1]. Technologies such as beamforming and integrated sensing and communications (ISAC) are crucial to enable mmWave communications. These technologies demand accurate bi-directional channel information in dynamic scenarios and use cases.

Bidirectional channel measurement and modeling have been performed in literature with aim to characterize the angle-of-arrival (AoA), angle-of-departure (AoD), delay, and Doppler domain information. For example, Ref. [2] developed a multi-bounce channel model for vehicles-to-everything (V2X) networks based on bidirectional multipath components (MPCs) information extracted from measurement. However, the developed model is based on statistical parameterization without specific association to the scatterers' information on location and electromagnetic properties. Alternatively, ray tracing (RT) and ray launching (RL) have been developed and widely used in the last few decades to deterministically simulate MPCs with the input of specific radio propagation environment. These simulation tools are based on geometry optics and are efficient at predicting dominant specular MPCs. On the flip side, the characterization of the propagation process by

RT/RL can accurately extract the information of scatterers in the environment. For example, Ref. [3] proposed a geometry-based clustering algorithm to cluster the measured outdoor channel using RT with imperfect environment map. The clustered MPCs and the sketched objects in the environment are associated; but some objects, such as cars, were ignored. This can affect the matching of measurement and RT, since the car can be a strong reflector.

In this paper, we aim to associate the indoor environment scatterers with the measured 60 GHz radio channel using point cloud data that was captured by a light detection and ranging (LiDAR) sensor. Our main contributions and novelties include: 1) a LiDAR-assisted channel measurement has been conducted in a typical lecture-room environment, where the LiDAR and the channel sounder are time-space synchronized; 2) based on the point cloud scanned by LiDAR, the 3D environment is accurately reconstructed to support RT simulations. 3) A novel cluster association method is proposed by matching the MPC clusters estimated from the measured channel and the MPC clusters simulated from RT. Finally, the channel characteristics, such as multiple bounces and composite path loss parameters, are analyzed and concluded.

II. CHANNEL MEASUREMENT

A. Channel Sounder

The channel sounder generates a repeating 2047 bit pseudo-random (PN) codeword that has a chip rate of 2 GHz. Fig. 1 shows the sounder at the receiver (Rx) side. The Rx was mounted on a mobile robot, as shown in Fig. 1a. Among them, the Rx antenna array consists of 16 horn antennas and the beamwidth of each horn antenna is 22.5° , as shown in Fig. 1b. The Rx antenna array covers 360° in azimuth and 45° in elevation. Meanwhile, a LiDAR and a 360° panoramic camera are fixed above the array antenna. The radio channel sounder, LiDAR, and camera are synchronized. This means that the environment from Rx perspective is captured while recording the channel. The transmitter (Tx) antenna array is equipped with 8 horn antennas with the same parameters, limiting the azimuth field-of-view (FoV) to 180° while elevation FoV is still 45° . Further details of the channel sounder system are provided in [4], [5].

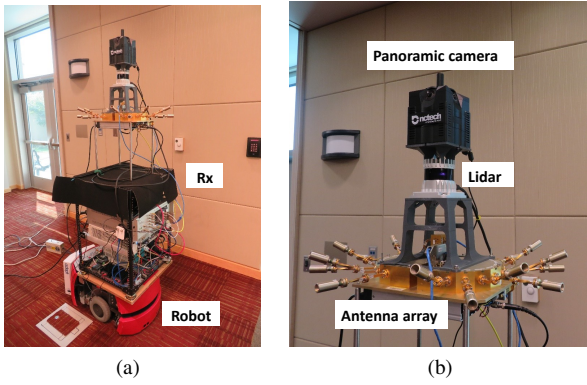


Fig. 1: (a) The channel sounder at Rx mounted on a robot. (b) Multi-sensor structure at Rx.

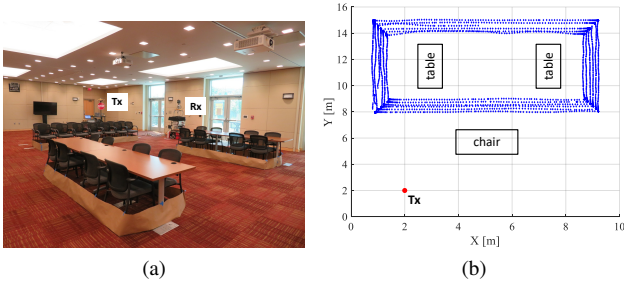


Fig. 2: (a) The measurement environment. (b) The positions of Tx and Rx (the blue dots are Rx positions during measurement).

B. Measurement Campaign

The measurement campaign was conducted in a typical lecture room, as shown in Fig. 2a. The heights of the Tx and Rx antenna arrays are 2 m and 1.48 m, respectively. Among them, Tx was fixed on a tripod and placed stationary on one corner of the room. Rx was carried by the robot and traveled in the planned route in the lecture room. The robot was equipped with a laser-guided navigational system, and reported the Rx positions in the environment through simultaneous localization and mapping (SLAM) algorithm. The position of Tx and the travel route of Rx are shown in Fig. 2b. The maximum velocity of the robot was 0.2 m/s, and the interval between each Rx position is about 10 cm. In addition, the line-of-sight (LOS) path was unobstructed throughout the measurement campaign. The space-alternating generalized expectation-maximization (SAGE) algorithm [6] is used to extract propagation paths and their parameters.

III. RAY TRACING ASSISTED CLUSTER ASSOCIATION PIPELINE

A. 3D Environment Reconstruction

As described in Section II-A, the channel sounder was measuring the channel while the LiDAR was recording environmental information. The environment is described by point cloud, as shown in Fig. 3a and Fig. 3b. Among them, the sparsity of the point cloud is exhibited. The locations where the points are sparse are further away from the observation point

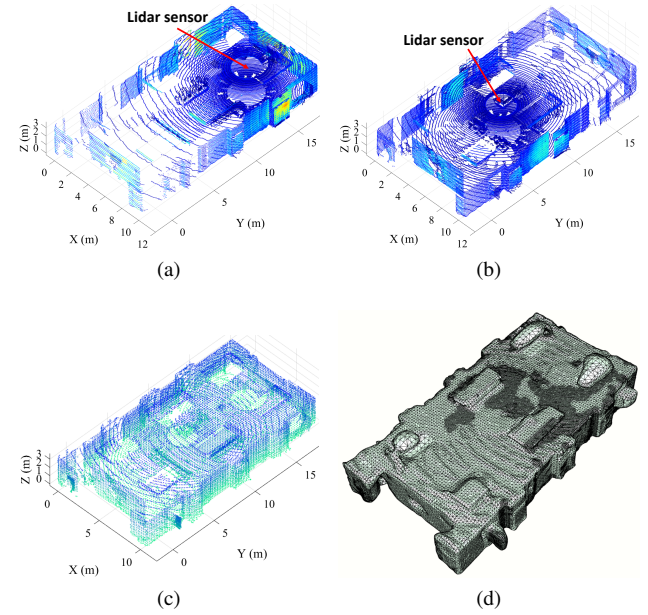


Fig. 3: Reconstruction 3-D environment. (a) Point cloud for snapshot one. (b) Point cloud for snapshot two. (c) Merged point cloud of snapshot one and two. (d) Meshed and reconstructed 3-D environment from the merged point cloud.

of the LiDAR, e.g., the points are more sparsely distributed on the left side of Fig. 3a and the right side of Fig. 3b. Therefore, firstly, we merge the point clouds to get a more comprehensive environment information, e.g., merging Fig. 3a and Fig. 3b leads to Fig. 3c. By carefully choosing the LiDAR locations, the merged point cloud exhibits a more uniform distribution over the space. Secondly, the screened Poisson surface reconstruction [7] is applied to the merged point cloud to reconstruct the environment geometry in Meshlab [8]. The meshed and reconstructed 3D environment is thus shown in Fig. 3d.

B. Ray Tracing

RT is performed to show the propagation process of MPCs. However, there are 200,000 triangles in the reconstructed environment. The complexity of RT simulation is high. Thus, RT based on the OptiX acceleration structure is adopted in this paper. Note that electromagnetic parameters of materials in the environment are unknown, which can cause the inaccurate power of simulated paths. That being said, we concern the propagation trajectory of paths from RT simulations (not the power), and the geometry parameters including delay, AoA, and AoD will be used for clustering. Since the Tx and Rx antenna arrays have limited field-of-view, as was mentioned in Section II-A, the MPCs beyond the field-of-view of the antenna array are removed from the RT results. The maximum number of bounce in RT is set to 3. This is because no reflection paths higher than the third order were observed from the measurement, which will be further elaborated in Section IV-A.

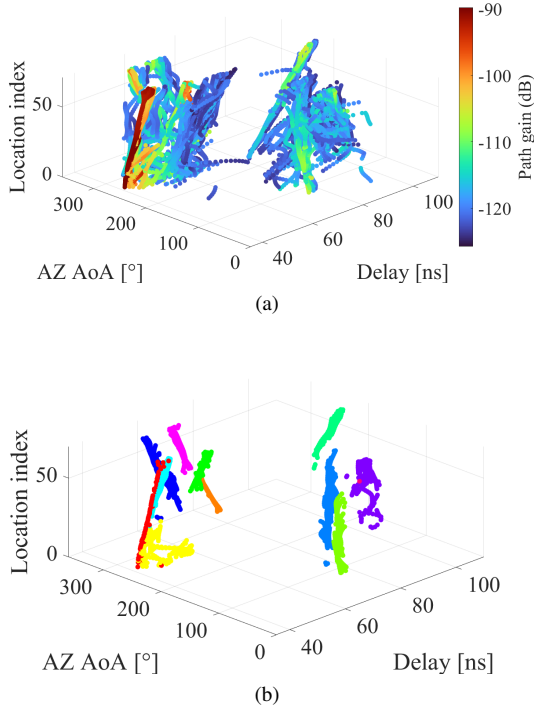


Fig. 4: Estimated MPCs from measurement and clustering results. (a) MPCs estimated from measured channel by SAGE. (b) MPC Clustering results. (Points with different colors represent different clusters.)

C. Clustering

For MPCs estimated from the measurement and MPCs simulated by RT, the density-based spatial clustering of applications with noise (DBSCAN) algorithm [9] is used to cluster them, respectively. DBSCAN groups together MPCs that are closely packed together. We use delay, azimuth AoA, and location to cluster the measured MPCs [10]. In this way, we can exploit the spatial continuity of MPC clusters to filter ghost paths in the measurement. Some MPCs that are discontinuously distributed in space will be treated as ghost paths and removed. In addition, adding the location domain to the clustering can also show spatial consistency. Fig. 4a and Fig. 4b show the measured MPCs and the corresponding clustering results using the DBSCAN algorithm, respectively. It is found that most ghost paths are removed and the generated clusters have good spatial consistency.

D. Cluster Association Between Measurement and Ray Tracing

In order to obtain the interaction objects of clusters in the reconstructed 3D environment, the MPCs clusters of RT and that of the measurement need to be associated. The association problem can be transformed into the 'assignment' problem and solved by matching using Hungarian algorithm or Kuhn-Munkres algorithm. These algorithms are able to find the minimized-weight perfect matching in a bipartite graph of a general assignment problem. These algorithms have been used in cluster tracking [11], [12]; however, they cannot obtain good

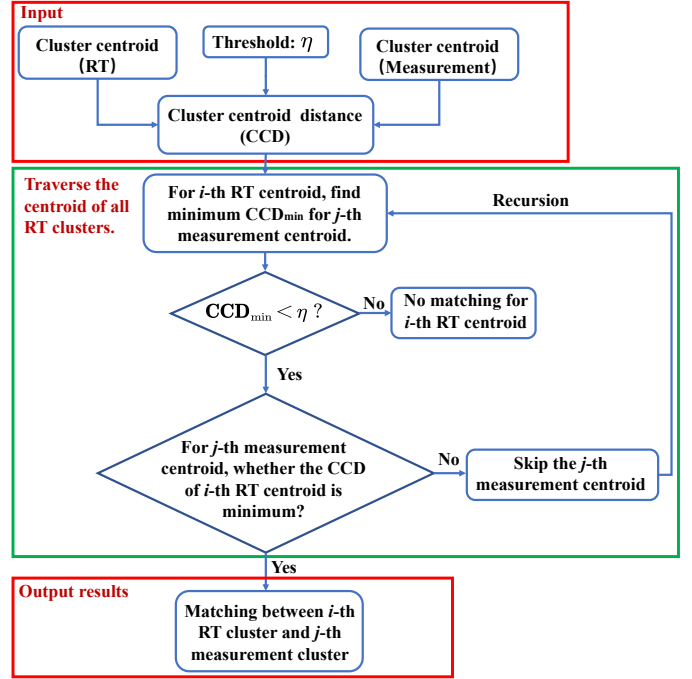


Fig. 5: The flowchart of proposed CCD threshold-based cluster association algorithm between RT and measurement.

results in cluster association. On the one hand, the association of clusters between RT and measurement cannot be abstracted into a bipartite graph, because some MPCs are only found in RT and some only in measurement, and these MPCs should not be matched. On the other hand, the Hungarian algorithm only finds the matches that minimize the weight among all clusters, rather than an optimal match for each cluster.

Therefore, we propose a cluster centroid distance (CCD) threshold-based association algorithm to find the optimal match for each cluster. The CCD is defined as

$$CCD_{i,j}^m = \sqrt{[C_{RT}^m(i) - C_{Mea}^m(j)]^2} \quad (1)$$

where $C_{RT}^m(i)$ and $C_{Mea}^m(j)$ are the i -th cluster centroid from RT and the j -th cluster centroid from measurement for parameter m , respectively. Parameter m represents the MPCs parameter category, such as delay and AoA. The CCD for all parameters are then obtained as

$$CCD_{i,j} = \sum_{m=1}^M N(CC D_{i,j}^m) \quad (2)$$

where $N(\cdot)$ is the normalized operation that is used to adjust different parameters to the same scale, and it is defined as

$$N(d) = \frac{d - d_{\min}}{d_{\max} - d_{\min}}. \quad (3)$$

In this paper, the delay and azimuth AoA of MPCs parameters are used to calculate CCD matrix, and $M = 2$.

Based on the obtained CCD for all parameters, cluster association between measurement and RT is performed, and the flowchart of proposed association algorithm is elaborated

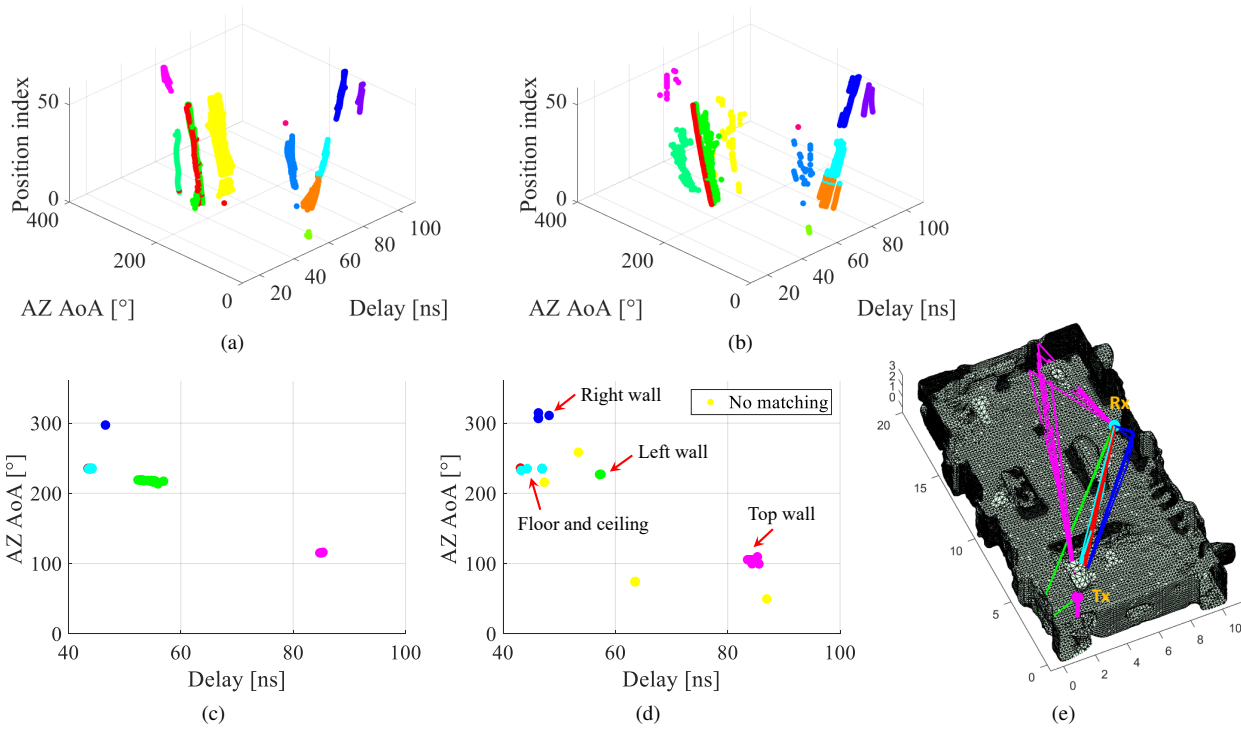


Fig. 6: The association results between measurement and RT. (a) Measured MPCs clustered in different colors across different Rx locations. (Red cluster represent LOS paths) (b) RT simulation and association results. (c) Measured MPCs clustered in different colors at Rx16 location. (d) associated RT clusters at Rx16 location. (e) 3D environment and associated rays at Rx16 location.

in Fig. 5. For i -th RT cluster, the closest measurement cluster j is determined by finding the cluster centroid with minimum CCD. If the minimum CCD is larger than the pre-defined threshold η , i -th RT cluster has no matching measurement cluster. When the minimum CCD is less than η , checking whether the i -th RT cluster centroid has minimum CCD among all RT cluster for j -th measurement cluster centroid. If true, the i -th RT cluster and the j -th measurement cluster will be matched as an associated cluster. Otherwise skipping the j -th measurement cluster and using the same steps to recursively search until a matching measurement cluster is found or all measurement clusters are searched. The value of pre-defined threshold η is smaller than the radius (epsilon) of the DBSCAN clustering. In this paper, we set $\eta = 0.025$ to obtain reasonable matching results.

Fig. 6 shows the clustering association results. Clusters with the same color in Fig. 6a and Fig. 6b indicate that they are matched and associated. It is found that most clusters and MPCs are associated. Fig. 6c and Fig. 6d show the association results for a single snapshot at the Rx16 location, where all measured clusters are matched by RT clusters. The yellow dots indicate unmatched RT clusters or MPCs in Fig. 6d. These clusters were not observed in the measurement, and they will be ignored in subsequent analysis. In addition, the rays in Fig. 6e are given in the same colors of corresponding clusters as in Fig. 6d. The intersection points of each ray in the associated cluster can thus be obtained.

Following the pipeline from Section III-A to III-D, the interaction objects in the 3D environment are associated to the corresponding MPC clusters of the measured radio channel, automatically.

IV. CHANNEL CHARACTERISTICS

A. Multiple Bounce Order

Based on the association results, the propagation process of clusters in the measurement is reproduced. The number of bounces for the measurement clusters can be obtained from the associated RT clusters. Fig. 7 shows the power percentage for paths of different number of bounces. Clearly, the LOS paths contribute most of the power in the channel. Meanwhile, one and two bounces also contribute power. Intuitively, one bounce contributes more power; but, interestingly, the contribution of paths of two bounces is more significant than that of one bounce in some snapshots. This is because the lecture-room environment is a closed cavity, and it provides conditions for multiple bounces of MPCs, and the propagation of paths of two bounces is less blocked in some locations/snapshots. In addition, it is found that most of the snapshots do not have three bounces components. The paths of three bounces are only observed in few snapshots, and their power percentage is very low. On the flip side, multiple bounces result in higher power decay, which makes it harder to be detected by channel sounder; it was reasonable to set the maximum number of bounce for RT to 3 in Section III-B.

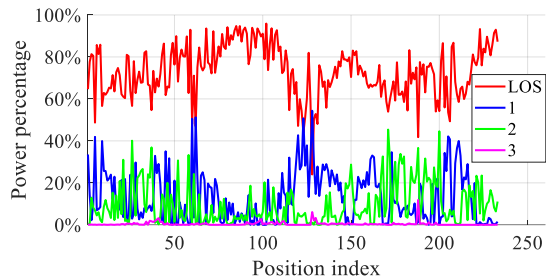


Fig. 7: The power percentage for different number of bounces.

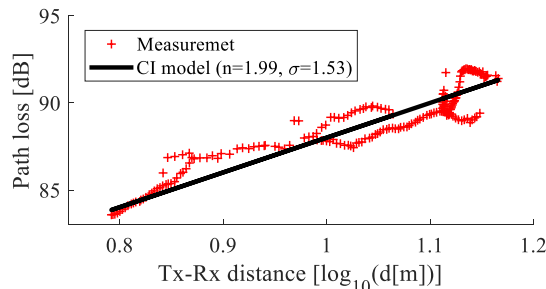


Fig. 8: Path loss and fitting results using CI model.

B. Composite Path Loss Parameters

According to the MPCs extraction results, the path loss at the k th position can be calculated [13]. The close-in (CI) free-space reference distance path loss model [14] can be exploited as a benchmark:

$$PL^{CI}(f, d)[\text{dB}] = \text{FSPL}(f, d_0)[\text{dB}] + 10n \log_{10}\left(\frac{d}{d_0}\right) + \chi_{\sigma}^{CI}, \text{ where } d \geq d_0$$

where f is the center frequency in gigahertz, d_0 is the close-in free-space reference distance and is set to 1 m, n denotes the path loss exponent (PLE), and χ_{σ}^{CI} is a zero-mean Gaussian random variable with a standard deviation σ in decibels. Fig. 8 illustrates the path loss and the fitting result using the CI model. It is found that the n of the measurement is slightly lower than that of the free-space propagation ($n = 2$); this is because the multiple bounces of MPCs contributed sufficiently to the received power.

V. CONCLUSION

In this paper, we presented a novel pipeline to associate the MPC clusters of a radio channel measured at 60 GHz to the 3D environment. The 3D environment is accurately reconstructed using point cloud scanned by LiDAR, and the RT simulation is conducted using the reconstructed 3D environment. A novel method to associate the clusters from the measurement and that from RT is proposed. Clustering using DBSCAN algorithm is performed for measurement and RT separately; the novel cluster association is then performed using the cluster centroid distance and recursive matching algorithm. Our proposed pipeline/method enables to associate the MPC clusters of measured channel to the interaction objects in the environment, automatically. We also demonstrated the multiple bounces and composite path loss parameters of the radio channel based

on the association results. The association results can more precisely calibrate RT material parameters in future work.

ACKNOWLEDGMENT

The authors would like to thank Dr. Xuesong Cai from Lund University for the help in clustering.

REFERENCES

- [1] C. De Lima, D. Belot, R. Berkvens, A. Bourdoux, D. Dardari, M. Guillaud, M. Isomursu, E.-S. Lohan, Y. Miao, A. N. Barreto, M. R. K. Aziz, J. Saloranta, T. Sanguanpuak, H. Srieddeen, G. Seco-Granados, J. Sututala, T. Svensson, M. Valkama, B. Van Liempd, and H. Wymeersch, "Convergent communication, sensing and localization in 6G systems: An overview of technologies, opportunities and challenges," *IEEE Access*, vol. 9, pp. 26 902–26 925, 2021.
- [2] C. Huang, R. Wang, P. Tang, R. He, B. Ai, Z. Zhong, C. Oestges, and A. F. Molisch, "Geometry-cluster-based stochastic MIMO model for vehicle-to-vehicle communications in street canyon scenarios," *IEEE Transactions on Wireless Communications*, vol. 20, no. 2, pp. 755–770, 2021.
- [3] G. Zhang, X. Cai, G. Fr, W. Fan *et al.*, "Geometry-based clustering characteristics for outdoor measurements at 28-30 ghz," *IEEE Antennas and Wireless Propagation Letters*, 2022.
- [4] R. Sun, P. B. Papazian, J. Senic, Y. Lo, J.-K. Choi, K. A. Remley, and C. Gentile, "Design and calibration of a double-directional 60 GHz channel sounder for multipath component tracking," in *2017 11th European Conference on Antennas and Propagation (EUCAP)*, 2017, pp. 3336–3340.
- [5] S. Blandino, J. Senic, C. Gentile, D. Caudill, J. Chuang, and A. Kayani, "Markov multi-beamtracking on 60 GHz mobile channel measurements," *IEEE Open Journal of Vehicular Technology*, vol. 3, pp. 26–39, 2022.
- [6] K. Hausmair, K. Witrisal, P. Meissner, C. Steiner, and G. Kail, "SAGE algorithm for UWB channel parameter estimation," in *COST 2100 Management Committee Meeting*. . ., 2010, pp. 1–7.
- [7] M. Kazhdan and H. Hoppe, "Screened poisson surface reconstruction," *ACM Trans. Graph.*, vol. 32, no. 3, jul 2013.
- [8] P. Cignoni, M. Callieri, M. Corsini, M. Dellepiane, F. Ganovelli, and G. Ranzuglia, "MeshLab: an Open-Source Mesh Processing Tool," in *Eurographics Italian Chapter Conference*, V. Scarano, R. D. Chiara, and U. Erra, Eds. The Eurographics Association, 2008.
- [9] M. Ester, H.-P. Kriegel, J. Sander, X. Xu *et al.*, "A density-based algorithm for discovering clusters in large spatial databases with noise." in *kdd-96 Proceedings*, vol. 96, no. 34, 1996, pp. 226–231.
- [10] N. Varshney, J. Wang, C. Lai, C. Gentile, R. Charbonnier, and Y. Corre, "Quasi-deterministic channel propagation model for an urban environment at 28 GHz," *IEEE Antennas and Wireless Propagation Letters*, vol. 20, no. 7, pp. 1145–1149, 2021.
- [11] C. Lai, R. Sun, C. Gentile, P. B. Papazian, J. Wang, and J. Senic, "Methodology for multipath-component tracking in millimeter-wave channel modeling," *IEEE Transactions on Antennas and Propagation*, vol. 67, no. 3, pp. 1826–1836, 2019.
- [12] C. Huang, A. F. Molisch, Y.-A. Geng, R. He, B. Ai, and Z. Zhong, "Trajectory-joint clustering algorithm for time-varying channel modeling," *IEEE Transactions on Vehicular Technology*, vol. 69, no. 1, pp. 1041–1045, 2020.
- [13] X. Cai, G. Zhang, C. Zhang, W. Fan, J. Li, and G. F. Pedersen, "Dynamic channel modeling for indoor millimeter-wave propagation channels based on measurements," *IEEE Transactions on Communications*, vol. 68, no. 9, pp. 5878–5891, 2020.
- [14] S. Sun, T. S. Rappaport, T. A. Thomas, A. Ghosh, H. C. Nguyen, I. Z. Kovács, I. Rodriguez, O. Koymen, and A. Partyka, "Investigation of prediction accuracy, sensitivity, and parameter stability of large-scale propagation path loss models for 5G wireless communications," *IEEE Transactions on Vehicular Technology*, vol. 65, no. 5, pp. 2843–2860, 2016.